International Journal of Solids and Structures xxx (2013) xxx–xxx

Contents lists available at SciVerse ScienceDirect

International Journal of Solids and Structures

journal homepage: www.elsevier.com/locate/ijsolstr

Non-local modeling of epoxy using an atomistically-informed kernel

Susanta Ghosh, Abhishek Kumar, Veera Sundararaghavan *, Anthony M. Waas

Department of Aerospace Engineering, University of Michigan, Ann Arbor, United States

ARTICLE INFO

Article history:
Received 3 December 2012
Received in revised form 25 March 2013
Available online xxxx

Keywords:
Non-local elasticity
Molecular dynamics
Simulation
Epoxy
Polymer

ABSTRACT

An integral type non-local continuum model for epoxy, used as the matrix material in aerospace structural composites, is developed from phonon dispersion data. Non-local continuum models can be used to regularize the stress fields at crack tips and molecular defect cores (e.g. disclinations in epoxies) where local (classical) elasticity theories fail to give bounded solutions. Integral type non-local elastic models phenomenologically incorporate microstructure information through a weighting function known as a kernel function. The kernel functions are typically obtained by matching dispersion curves computed using lattice dynamics. However, the use of lattice dynamics for amorphous polymers that do not have an underlying lattice structure is computationally prohibitive. In this paper, a molecular dynamics based approach is used for the computation of the non-local kernel, for amorphous epoxy. Dispersion relations calculated from the reciprocal-space velocity–velocity autocorrelation function are used to build the kernels. The computed atomistic kernel is used to predict stress solutions for some example problems where classical elasticity predicts singularities.

1. Introduction

Fundamental physical laws based on classical solid mechanics assume a continuum description where the length-scales are much larger than inter-atomic distances. Consequently, classical continuum models, which are local by construction, are of limited use in capturing phenomena where nano-scale interactions influence the outcome of a problem, for example, at crack-tips and at dislocation cores (Eringen, 2002; Askes and Aifantis, 2011; Kunin, 1982). In view of these, quasi-continuum (QC) methods have been developed to communicate information from one scale to the other efficiently (Tadmor et al., 1996; Miller and Tadmor, 2009; Tan et al., 2008). In these methods, certain key regions are modeled atomistically while the rest are modeled using finite element techniques and hence requires a fraction of computational cost compared to a full atomistic model. There are other kinds of QC methods where the continuum energy densities are obtained from interatomic interactions (Zhang et al., 2004; Arroyo and Belytschko, 2002). Though other atomistic based continuum schemes are used for epoxy and epoxy nano-composites (Jiang et al., 2007), QC methods have been used mostly to solve problems for crystalline structure (on the atomistic scale). To the best of our knowledge, QC or other similar methods (Hakobyan et al., 2012) have not been used to simulate amorphous structures such as epoxy. Classical elasticity models describe reversible and local behavior. Thus, stresses at a point are considered to depend purely upon the strain at that point. In contrast, molecular models are inherently non-local where stresses at an atom are affected by interactions with several atoms within a finite volume centered at that atom. In recent work, we showed that the long-range nature of inter-atomic forces affect the degree of non-locality that needs to be considered in continuum theories (Sundararaghavan and Waas, 2011). Different continuum theories have been proposed to incorporate such nonlocal effects, and these can be classified into either an integral-based description or a higher order gradient based description. The integral-based description represents the nonlocal stress at a point as a weighted integral of the local stresses through a nonlocal kernel (Eringen and Edelen, 1972, 1987; Eringen, 1972; Eringen et al., 1977). A similar nonlocal integral-based approach, based on displacements rather than stresses, arise in peridynamic formulations (Silling, 2000). Gradient based elasticity theories can be seen as a variation of the integral formulation. It can be shown that the first order stress gradient theory or the strain gradient theory corresponds to a specialized kernel within the integral based formulation (Eringen, 1983; Aifantis, 1992; Ru and Aifantis, 1993; Gutkin and Aifantis, 1996, 1999). A key feature of the integral-based nonlocal theory is the use of a non-local kernel. This non-local description is seen to eliminate singularities found in classical elasticity near discontinuities (such as cracks) and defects (such as disclinations), since it encompasses a characteristic length scale that can be associated with the description of the material nanostructure – different nanostructures lead to different characteristic length scales. As first shown in Eringen (1972), the non-local kernel can be calibrated using atomistic simulations, typically by

* Corresponding author. Tel.: +1 7346157242.
E-mail addresses: veeras@umich.edu (V. Sundararaghavan), dcw@umich.edu (A.M. Waas).

0020-7683/$ - see front matter © 2013 Elsevier Ltd. All rights reserved.
http://dx.doi.org/10.1016/j.ijsolstr.2013.04.025

matching phonon dispersion curves predicted by the atomistic model with similar prediction from the non-local theory. This approach has been demonstrated for crystalline metals (with simple lattices) and quasi-1D materials such as nanotubes (DiVincenzo, 1986; Ilcewicz et al., 1986; Picu, 2002; Maranganti et al., 2007; Sundararaghavan and Waas, 2011).

However, non-local kernels of integral type nonlocal formulations for amorphous materials (e.g. thermoset polymers) are yet to be established. In this work, we consider polymers such as epoxy that are used as matrix materials in the aerospace industry. The use of lattice dynamics for prediction of phonon dispersion in epoxies is computationally tedious due to the need for large simulation cells to capture the amorphous nature. Recently, there have been some notable studies to capture size effects in polymeric materials via experiments (Lam et al., 2003; Han, 2010). However, they do not predict the parameters for non-local elasticity.

Molecular Dynamics (MD) simulations are routinely used for epoxy systems. For instance, interface debonding problem between epoxy and silica in a multi-layered material system have been previously studied using atomistic simulations (Bykztrk et al., 2011; Lau et al., 2012). In our recent work (Sundararaghavan and Kumar, 2013), atomistic simulations were used to identify both the chemistry and geometry involved in molecular mechanism of compressive yielding in epoxies. In this work, dispersion relations are calculated from the velocity–velocity autocorrelation function in the reciprocal space directly from the results of the molecular simulation, following the method proposed in Dickey and Paskin (1969), and also used in Heino (2007). The results are used to predict the non-local kernel for amorphous DGEBA/DDS epoxy structure. Using the non-local kernel, we study the stress fields where non-local interactions are prominent and classical elasticity provides singular solutions. Two cases are considered in the context of addressing the singular solutions arising in local elasticity; (i) a case of a Griffith crack in an epoxy matrix and (ii) a case of a wedge disclination within the epoxy matrix. The paper is arranged as follows. Section 2 describes the nonlocal elastic model and the strategy to extract the nonlocal stresses from local ones. In the Section 3, the detailed atomistic modeling of epoxy is described. Section 4 describes the dispersion data and an appropriate kernel fit to this data. It also provides a numerical estimate of stress fields for few example problems where local elasticity gives singular solutions.

2. Nonlocal elasticity

2.1. Background theory

The balance law for nonlocal linear elastic solids is given by Eringen (1983):

$$t_{kl,k} + \rho(f_l - \dot{v}_l) = 0 \quad \text{in volume } V \tag{1}$$

Here, ρ and $\boldsymbol{f}$ are the density and the body force per unit mass, V is the volume of the body. $\boldsymbol{t}$ is the nonlocal stress tensor, which is symmetric $t_{kl} = t_{lk}$. The boundary condition for a nonlocal elastic body can be written as:

$$t_{lk}(\boldsymbol{x})\, n_l = p_k(\boldsymbol{x}), \quad \boldsymbol{x} \in S_s \tag{2}$$

$$u_k(\boldsymbol{x}) = u_k^0(\boldsymbol{x}), \quad \boldsymbol{x} \in S_d \tag{3}$$

Where, p denoted the surface traction field. u^0 denotes prescribed displacement. S_s and S_d denote boundaries where stresses and displacements are prescribed.

For isotropic materials (such as thermoset epoxies considered here), the nonlocal stress, t_{kl}, can be described using a single kernel function (α) as,

$$t_{kl}(\boldsymbol{x}) = \int_\Omega \alpha(\|\boldsymbol{x} - \boldsymbol{x}'\|)\sigma_{kl}(\boldsymbol{x}')\, d\Omega \tag{4}$$

Here, $\boldsymbol{\sigma}$ is the Hookean stress tensor, $\boldsymbol{x}$ and $\boldsymbol{x}'$ are position vectors for two material points in Ω. Ω is the compact support in V for the kernel. The kernel function, α, has the following property

$$\int_\Omega \alpha(\|\boldsymbol{x} - \boldsymbol{x}'\|)\, d\Omega = 1 \tag{5}$$

Consequently, α reverts to a delta function as the zone of influence vanishes which leads to classical (local) elasticity. Furthermore, α peaks at $\|\boldsymbol{x} - \boldsymbol{x}'\| = 0$ and generally decays with increasing $\|\boldsymbol{x} - \boldsymbol{x}'\|$. Recent research has indicated that the kernel need not be always positive and the decay need not be monotonous (Picu, 2002; Sundararaghavan and Waas, 2011). It is noted that the balance law is an integro partial differential equation and solving this equation for an arbitrary kernel is difficult. In the present work, the integro partial differential equation is transformed to a partial differential equation following Eringen (Eringen, 1983), and described in Section 2.2.

The primary issue with non-local elasticity is the computation of a physically valid kernel function, using an appropriate sub-scale model, which has only been demonstrated so far with idealized crystalline solids or at zero temperature (molecular statics). The classical approach (suggested by Eringen (2002)) for reconstructing the non-local kernel is to match the dispersion curves of plane waves predicted by the non-local theory with dispersion curves calculated from a sub-scale atomistic model. Dispersion curves of a 1-D axial rod model are calculated by using displacement $u(x,t)$ of the plane wave form $u(x,t) = Ue^{i(kx-\omega(k)t)}$ (where k is the wavenumber[1] and $\omega(k)$ denotes the frequency of the plane wave) in the 1-D governing equation $\frac{\partial \sigma}{\partial x} = \rho \frac{\partial^2 u}{\partial t^2}$. For an isotropic linear elastic solid with Young's modulus (E) and density (ρ) with speed of sound (in the continuum limit) given as $c = \sqrt{\frac{E}{\rho}}$, this leads to the well-known formula

$$\frac{\omega}{c} = k\sqrt{\hat{\alpha}(k)} \tag{6}$$

where $\hat{\alpha}(k)$ represents the Fourier transform of α.[2] For a three-dimensional isotropic solid (e.g. epoxy matrix), the Fourier transform of Eqs. (1) and (4) will give the following equation for the dispersion curve:

$$\omega_j(k)/c_j = k\sqrt{\hat{\alpha}(k)}, \quad j = 1,2 \tag{7}$$

where c_1 and c_2 are the phase velocities of the longitudinal and transverse waves. The dispersion curve (ω_j versus k) obtained from atomistic simulations can be used to compute the non-local kernel $\hat{\alpha}(k)$ directly using the above equation.

2.2. Green's function approach

The following paragraph describes the steps to reduce the integro-partial differential equation (1) for non-local elasticity to a partial differential equation, under a suitable set of assumptions. This strategy was proposed in Eringen (1983) and subsequently used for many problems. This idea is motivated by the fact that the integro-partial differential equations are difficult (or impossible) to solve in closed form, whereas, the reduced partial differential equations would be easier to handle or their solutions are already known from classical elasticity. The intended nonlocal solution can be subsequently obtained from the solutions of the reduced partial differential equation. Let $\alpha(r)$ be the Green's function for the operator L, *i.e.*

$$L\alpha(r) = \delta(r) \quad \text{where } r = \|\boldsymbol{x} - \boldsymbol{x}'\| \tag{8}$$

[1] i.e. the number of wavelengths per 2π units of distance.

[2] $\hat{\alpha}(\boldsymbol{k}) = \int_{\mathbb{R}^n} \alpha(\boldsymbol{x}) e^{-i\boldsymbol{x}\cdot\boldsymbol{k}} dV_x$.

Please cite this article in press as: Ghosh, S., et al. Non-local modeling of epoxy using an atomistically-informed kernel. Int. J. Solids Struct. (2013), http://dx.doi.org/10.1016/j.ijsolstr.2013.04.025

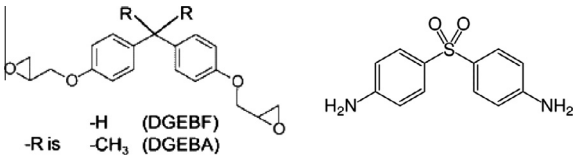

Fig. 1. Chemical structure of epoxy resin. DGEBA and the amine monomer 4-4′ diamino diphenyl sulfone employed in this work.

Then the application of L on Eq. (4) yields,

$$Lt_{kl} = \sigma_{kl} \tag{9}$$

Differentiating both sides

$$(Lt_{kl})_{,k} = (\sigma_{kl})_{,k} \tag{10}$$

If the operator L has constant coefficients[3] then it reduces to

$$Lt_{kl,k} = \sigma_{kl,k} \tag{11}$$

Using the above relation, the balance law of Eq. (1) can be written as

$$\sigma_{kl,k} + L(\rho(f_l - \ddot{u}_l)) = 0 \tag{12}$$

If the condition $L(\rho(f_l - \ddot{u}_l)) = 0$ is satisfied then the above equation reduces to the classical equilibrium equation: $\sigma_{kl,k} = 0$. The operator L can also be applied to the non-local traction boundary conditions (Eq. (2)), if specified. This sets up a local boundary value problem for which the solution is well known through either analytical or numerical (finite element analysis) means. Subsequently Eq. (4) would be used to retrieve the nonlocal stress for the problem.

The key input to this approach is the operator L which needs to be computed from fine scale simulations such as lattice dynamics or molecular dynamics. Recall that the kernel function ($\hat{\alpha}$) is obtained in the frequency domain from the atomistic dispersion curve (Eq. (7)) as described in the previous section. The operator $\hat{L}$ can be obtained by taking a Fourier transform of Eq. (8) which leads to a simple relation: $\hat{L}\hat{\alpha} = 1$. In other words, the Fourier transformed operator $\hat{L}$ is simply the inverse of the fourier transformed kernel function: $\hat{L} = 1/\hat{\alpha}$. There could be several ways to approximate the Fourier transformed kernel ($\hat{\alpha}$ of Eq. (7)) from simulation data. Popular choices are simple polynomials (Eringen, 2002) and exponential functions (Sundararaghavan and Waas, 2011). For example, the stress gradient theory with one nonlocal-parameter, ℓ, is of the form,

$$(1 - \ell^2\nabla^2)t_{kl} = \sigma_{kl} \tag{13}$$

Here, the operator is

$$L = (1 - \ell^2\nabla^2) \quad \text{and} \quad \hat{\alpha} = \frac{1}{\hat{L}} = \frac{1}{(1 + \ell^2 k^2)} \tag{14}$$

The corresponding kernels in 1-D can be obtained by inverse Fourier transform of the above:

$$\alpha(r) = \frac{1}{2\ell}e^{-r/\ell}, \quad r = |x - x'|, \quad x, x' \in V \subset \mathbb{R} \tag{15}$$

The steps to obtain the material specific kernel, α, through MD simulation is described in the next section.

[3] The assumption is valid for small deformation. Note that the kernel function changes with strain under finite deformation. Thus, in general, L may not have constant coefficients.

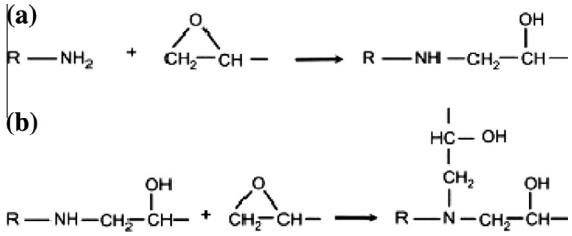

Fig. 2. Epoxy-amine cross linking through reaction of amine group with epoxide group.

3. Molecular dynamics simulation for epoxy

For this study, a common epoxy was employed: Di-Glycidyl Ether of Bisphenol A (DGEBA). The epoxy and amine monomer structures are shown in Fig. 1. The epoxy molecules were cross-linked (cured) with 4-4′ diamino diphenyl sulfone (DDS). Each epoxy monomer has two epoxide (oxirane ring) groups, each with a cross-linking functionality of one towards amine curing agents, for a total functionality of two; each DDS monomer has two amine groups, each with a functionality of two towards epoxy molecules, for a total functionality of four. The typical synthetic epoxy to amine stoichiometric ratio is approximately 2:1 or 33.3 mol% amine. Fig. 2 shows polymer formation driven by the bonding of epoxide group in DGEBA and the amine groups in DDS. During formation of a cross-link, the primary amine group reacts with epoxide group forming a bond between nitrogen of DDS and the terminal carbon of the epoxide group. The carbon–oxygen bond breaks between the terminal carbon and the epoxide oxygen forming an alcohol (-OH) link. The cross-linked structure in Fig. 2(a) can undergo further reaction with another epoxy molecule forming a cross-linked molecular structure (Fig. 2(b)).

Materials Studio software (Accelrys, 2007) was used to build a dendrimeric structure with 36 amine groups and 71 epoxy groups resulting in a total of 4601 atoms. The method for formation of cross linked structure was based on the work of Christensen (2007). In this approach, the thermoset resin is modeled by starting with a single monomer and then cross-linking a second layer of monomers around it. In the next step, a third layer of monomers are cross-linked to the second layer. In this way, generations (layers) of monomers are added to a seed structure that grows in size at every pass. The principal advantages of the dendrimer growth method are the complete avoidance of artificial network strain during curing and the low computational cost of the growing procedure. In the initial dendrimer, 75% of available epoxy sites were cross-linked which is representative of many structural epoxies (Wang et al., 2003). For all simulations presented in this study, CVFF (Consistent Valence Force Field) potential (Dauber-Osguthorpe et al., 1988) was used for bonded as well as non-bonded interactions. This force-field successfully predicted accurate thermodynamic properties of interest for epoxies in a previous study (Varshney et al., 2008). To model the equilibrated structure, the initial dendrimer structure was first optimized by minimizing the energy of the structure using 10,000 iterations of a conjugate gradient (CG) minimizer. Subsequently, molecular dynamics was performed over several annealing cycles. Each annealing cycle involved a NPT simulation at very low temperature (1 K) followed by another NPT run at 600 K (which is above glass transition temperature $T_g \approx 425$–495 K for DGEBA/DDS (Tcharkhtchi et al., 2000)). The sides of the cell and density for each annealing cycle are provided in Fig. 3. These simulations were performed at 1 atm pressure for 10,000 steps each (at 1 fs time step). The density was tracked over successive anneal cycles until convergence was seen. A final density of 1.17 g/cc at 1 K and 1 atm pressure was

Please cite this article in press as: Ghosh, S., et al. Non-local modeling of epoxy using an atomistically-informed kernel. Int. J. Solids Struct. (2013), http://dx.doi.org/10.1016/j.ijsolstr.2013.04.025

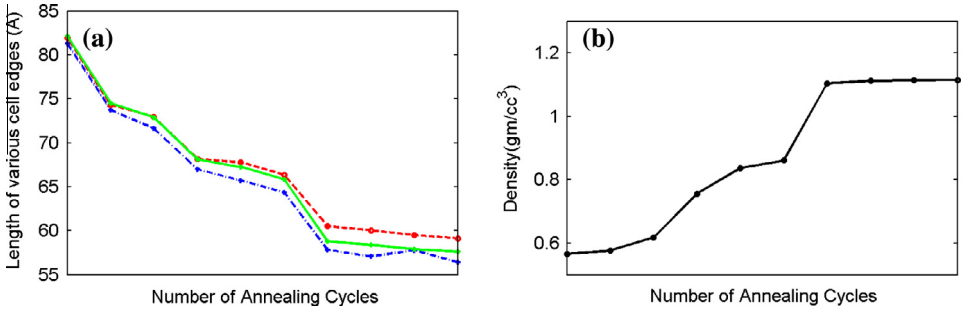

Fig. 3. (a) Length of cell sides and (b) density for successive annealing cycles.

obtained (see Fig. 3(a)). The elastic stiffness tensor of the optimized epoxy structure was found to be isotropic, as expected, with an elastic modulus of 4.83 GPa and a Poisson's ratio of 0.33. The thermal expansion coefficient between 223 K and 323 K is measured to be 54.6 μ/K, close to the value of 55 μ/K reported in experiments (Tcharkhtchi et al., 2000), for specific match see Fig. 4 of Sundararaghavan and Kumar (2013).

Dispersion relations are calculated based on velocity–velocity autocorrelation function in the reciprocal space as described in Heino (2007). Specifically, the vibrational spectrum for a given wavevector can be calculated as the Fourier transform of the autocorrelation function in reciprocal space. For a given polarization, $p = x, y, z$, the autocorrelation function is given by:

$$R^p_{\boldsymbol{k}}(t) = \frac{\langle v^p_{\boldsymbol{k}}(0) v^p_{\boldsymbol{k}}(t)\rangle}{\sum_{p=x,y,z}\langle v^p_{\boldsymbol{k}}(0) v^p_{\boldsymbol{k}}(0)\rangle} \tag{16}$$

$$v^p_{\boldsymbol{k}}(t) = \sum_{i=1}^{N_a} v^p_i(t)\, e^{-i\boldsymbol{k}\cdot\boldsymbol{r}_i(t)} \tag{17}$$

Here, $\boldsymbol{k}$ is the wave vector of interest, v^p_i is the pth component of the velocity of atom i, and $\boldsymbol{r}_i(t)$ is the position of atom i at time t. N_a is the total number of atoms in the MD simulation. As such, $v^p_k(t)$ is the reciprocal space representation of the velocity and $R^p_{\boldsymbol{k}}(t)$ its autocorrelation. By Fourier transforming $R^p_{\boldsymbol{k}}(t)$, the dominant frequencies for a given wave vector $\boldsymbol{k}$ can be found (see Appendix (A) for explanation). Typically sharp peaks are found in the frequency domain and the dispersion relation is determined from the locations of these peaks.

The approach was validated by comparing against experimentally measured dispersion curves of FCC copper system (see supplementary article attached to this paper). The key novelty in this work is the use of autocorrelation functions to directly compute the phonon dispersion curve from molecular dynamics data. This approach has not been studied previously. The approach has several advantages compared to other sub-scale models (e.g. density functional perturbation theory, lattice dynamics etc.) including the ability to compute phonon dispersion for complex amorphous cells and the ability to compute the phonon dispersion under realistic temperatures and strain states (although these aspects are not part of this work).

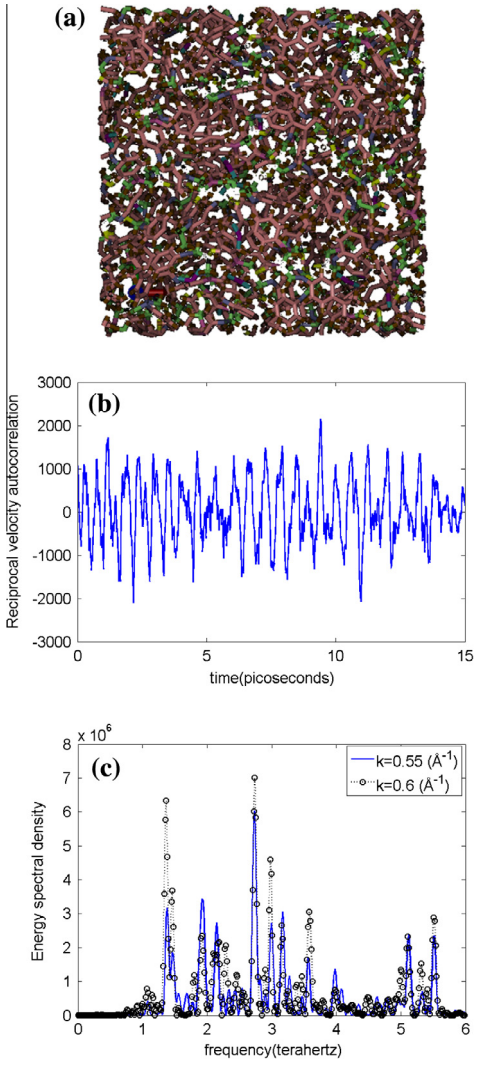

Fig. 4. Dispersion in epoxy (LAMMPS): (a) The optimized epoxy structure with 4500 atoms. The optimized structure has a density of 1.15 g/cc. The (b) autocorrelation, $A^p(k,t)$ for $k = 0.55$ and its (c) Fourier transform for $k = 0.55$ and 0.6 Å^{-1}. The dispersion curve can be computed by noting down the peak frequencies at each k-value.

4. Numerical results

In the following, we describe the phonon dispersion of epoxy and the process of fitting the non local kernel. The longitudinal and the two transverse modes of vibration in the epoxy were obtained from the results of a 30,000 time-step NVE simulation (at 1 fs time step). The phonon frequencies were computed using only the atoms that form the backbone of the epoxy chain (so that high frequency vibrations of protons are not included in the calculation). This also excludes the CH_3, double-bond O and OH groups attached to the chain backbone in Figs. 1 and 2. Data was obtained at 10 intervals from a wave vector (=$2\pi/\lambda$) of 0.15 to a wave vector of 1.5 Å^{-1}. While a perfect lattice gives sharp frequencies from which dispersion curves can be clearly identified, dispersion of an amorphous polymer may show several peak frequencies at one wavelength corresponding to the oscillations of various different atoms in the epoxy backbone (see Fig. 4). In order get a single

Please cite this article in press as: Ghosh, S., et al. Non-local modeling of epoxy using an atomistically-informed kernel. Int. J. Solids Struct. (2013), http://dx.doi.org/10.1016/j.ijsolstr.2013.04.025

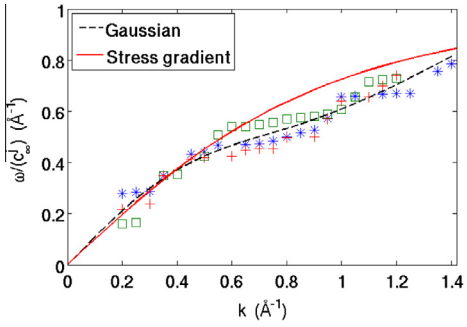

Fig. 5. Phonon dispersion data for epoxy. Data points marked by $*$ are for longitudinal mode of vibration, □ and + denote transverse modes.

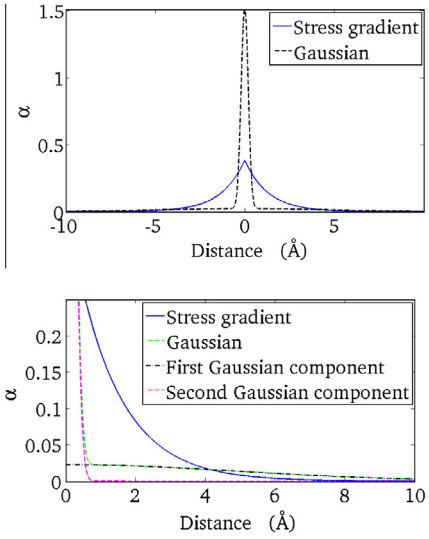

Fig. 6. (top) Different kernel functions obtained from phonon dispersion data. (bottom) Two different components of Gaussian kernel.

frequency data point to construct the dispersion curve, only the highest energy peaks are selected from the frequency versus spectral density of energy data for each wavenumber. The phonon dispersion data thus obtained is given in Fig. 5. Fig. 3 below shows the energy spectral density for two different wave vectors. It is evident that even though the locations of largest peaks are nearly identical, these are two widely different signals having multiple peaks. The data set was normalized with respect to the phase velocities computed at wave number 0.35 Å^{-1}, which accommodates exactly two wavelengths (in simulation box of 35.5 Å size). Note that for an isotropic material, the two transverse modes are expected to have identical wave dispersion. Secondly, the longitudinal and transverse wave dispersion is identical when normalized with the sound velocities (see Eq. (7), $\omega_j(k)/c_j = k\sqrt{\hat{\alpha}(k)}$). This is seen in Fig. 5. The trend of the dispersion curve is consistent with those reported in Chen and Lakes (1989) at low k for polymeric materials.

By fitting the stress gradient curve (Eq. 14) to the dispersion data, the nonlocal parameter was found to be $\ell = 1.2364$ Å. As plotted in Fig. 5, the single parameter stress gradient model is unable to capture the dispersion curve over the entire range of wave numbers. To get a better fit, higher order polynomials (e.g. $\alpha(k) = 1/(1 + \ell^2 k^2 + \ell_2^4 k^4)$) were attempted. However, it was found that these cannot reproduce the typical upward trend for larger k effectively. In order to provide a meaningful kernel fit to the dispersion data, several combinations of suitable functions may be used. In the present work, a sum of two Gaussian functions is considered, as also used in previous studies (Sundararaghavan and Waas, 2011). The kernel is given as,

$$\alpha(r) = \frac{1}{I_{1d}}\left(c_2 e^{-\frac{r^2}{c_3^2}} + c_4 e^{-\frac{r^2}{c_5^2}}\right), \quad I_{1d} = \sqrt{\pi}(c_2 c_3 + c_4 c_5), \quad r = |x - x'| \tag{18}$$

The Fourier transform of the kernel to be fitted to the atomistic data is given by,

$$\hat{\alpha}(k) = \frac{1}{I_{1d}}\left(c_2 c_3 \sqrt{\pi} e^{-\frac{c_3^2 k^2}{4}} + c_4 c_5 \sqrt{\pi} e^{-\frac{c_5^2 k^2}{4}}\right) \tag{19}$$

The kernel is normalized to have unit area in real space and it satisfies all the desired conditions mentioned in Section 2.1, hence it is expected to represent both local and nonlocal behavior effectively from the dispersion data. Furthermore, the use of multiple Gaussian functions is motivated by the need to better represent the shape of computed dispersion data. The least square best fit of the Fourier transformed kernel is plotted in Fig. 5. It shows that the Gaussian fitted kernel can capture the upward trend at larger k of the dispersion data while it can match the deviation from the $\omega/c_\infty = k$ line and subsequent moderate increase in frequency. Unlike the kernel given by Eq. 14 the Gaussian kernel can show change in curvature, which is apparent from the current data set. The parameter set obtained by best fit is $[c_i] = [0.0185, 6.9088, 1.2146, 0.2740]$. The kernel is plotted in Fig. 6, it is apparent that the two Gaussian components show different attenuations, pointing to the fact that these predict two scales of nonlocal effects. The shorter zone of influence has a higher amplitude and higher area under it. The Gaussian kernel with larger and smaller radii of influence have nonlocal weights 0.2662 and 0.7225 respectively, and the approximate radius of influence 1 and 10 Å respectively. The Gaussian kernel with larger radius of influence carries much smaller weight at the center compared to both Gaussian component with shorter radius of influence and the stress gradient kernels, but it overtakes the stress gradient kernel at about 4 Å.

Unlike the Gaussian kernel, the stress gradient kernel has one nonlocal parameter and can predict only one radius of influence, approximately 6 Å. Note that in Sundararaghavan and Waas (2011) such kernels have been used to capture the dispersion relation in a carbon nanotube by matching the phonon dispersion curves predicted by lattice dynamics to those predicted by the non-local elasticity theory. It was observed that the kernel changes sign close to the inflection point of the inter-atomic potential. Other sources (Picu, 2002) have also reported that the kernel is positive at the origin and changes sign after some distance. Their calculations for Aluminum glass shows that the sign change occurs between 2–2.5 Å. The sign change in their kernel is related to the sign change of the inter-atomic force at the inflection point of the inter-atomic potential and the relative arrangement of atoms. However, the current data set for the particular epoxy studied here does not show any negative contributions. The fact that $\hat{\alpha}$ is positive for all k indicates lack of any unstable deformation modes (Bazant and Chang, 1984). This condition is satisfied by both of the kernels obtained here.

The 2-D kernels in the real space for isotropic materials can be obtained from 1D kernels (Eq. (14) and (19)) in reciprocal space by invoking the axisymmetry condition. The 2D stress gradient kernel is defined as:

$$\alpha(r) = \frac{1}{2\pi\ell^2} K_0(r/\ell), \quad r = \|\boldsymbol{x} - \boldsymbol{x}'\|, \quad \boldsymbol{x}, \boldsymbol{x}' \in V \subset \mathbb{R}^2 \tag{20}$$

where, K_0 is the modified Bessel Function of the second kind of order zero (Abramowitz and Stegun, 1972).

Similarly the 2-D Gaussian kernel:

$$\alpha(r) = \frac{1}{I_{1d}}\left(\frac{c_2}{c_3\sqrt{\pi}} e^{-\frac{r^2}{c_3^2}} + \frac{c_4}{c_5\sqrt{\pi}} e^{-\frac{r^2}{c_5^2}}\right), \tag{21}$$

where, $r = \|\boldsymbol{x} - \boldsymbol{x}'\|, \quad \boldsymbol{x}, \boldsymbol{x}' \in V \subset \mathbb{R}^2$

Please cite this article in press as: Ghosh, S., et al. Non-local modeling of epoxy using an atomistically-informed kernel. Int. J. Solids Struct. (2013), http://dx.doi.org/10.1016/j.ijsolstr.2013.04.025

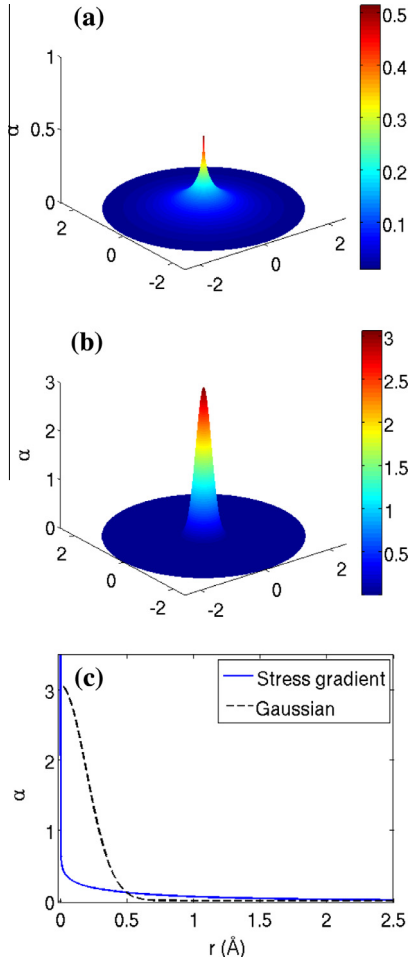

Fig. 7. 2-D kernels. Given by (a) Eq. (20) and (b) Eq. (21). Axes on the plane are in Å. (c) Radial profile.

The 2D kernels are plotted in Fig. 7(a) and (b). In contrast to the 1-D kernel described previously, the stress gradient kernel has a singularity at the center. The radial profiles for Gaussian kernel and stress gradient kernel are compared in Fig. 7(c). The singularity (at $r = 0$) for the 2D stress gradient kernel is seen in Fig. 7(a) and is more apparent in Fig. 7(c). Within a radial distance of 0.5 Å, the Gaussian kernel has nearly 70% of its weight, whereas stress gradient has only 13% weight. But this trend changes with distance, as the sharper component of the Gaussian kernel dies down quickly and the weights for the stress gradient overcomes the Gaussian. At around 2.72 Å they have the same weight, 76%. For even larger distances the stress gradient kernel attenuates much quickly, whereas the flatter component of the Gaussian kernel still contributes to a smaller extent. The implications of these differences in attenuation is described next in the context of a Griffith crack problem in epoxy matrix.

Since, neither of the kernels under consideration have compact support, the kernels were truncated after some specific radial distances from the center, which is defined as the *computational* radius of influence (r_{cutoff}). The volume covered by the radius of influence is the *computational* compact support (Ω^{comp}) of the kernel. The kernels were set to zero outside their compact support and scaled to satisfy the normalization condition inside their compact support. It is important to note that radii of influence are different in different dimensions for the same functional form of the kernel. There is no specific rule to select the radius of influence, however, it is customary to choose the radial distance from the central point to the point where the integral of the kernel reaches some specific value (w_{cutoff}) as the *computational* radius of influence. The computational kernel α^{comp} is given below:

$$\alpha^{\text{comp}}(r) = \frac{\alpha(r) - \alpha(r_{\text{cutoff}})}{(w_{\text{cutoff}} - \Omega^{\text{comp}}\alpha(r_{\text{cutoff}}))} \tag{22}$$

If the cutoff weight is chosen as 0.9, the corresponding radii of influences are 4 and 7 Å for the 2D Stress Gradient kernel and 2D Gaussian kernel respectively.

4.1. Griffith's crack problem

In the following, the *Griffith crack* problem is considered as an example to demonstrate the use of an atomistically informed nonlocal elasticity problem. The *Griffth crack* problem consists of a thin elastic plate, of thickness, t, with a slit crack of length $2L$, $L = 0.5$ μm, located at $-L \leqslant x \leqslant L$ on Y-axis, and subjected to a far field uniform tension σ_∞. The crack is assumed to be "mathematically sharp", implying a zero radius of curvature at the tip. The plate dimensions and slit crack length, L are much larger than the plate thickness, t. The 2D stress fields, corresponding to a classical plane stress continuum model are well known, and produces infinite stresses at the crack-tip for classical elasticity.

The stress field via classical elasticity is given below:

$$\sigma_{22} = \sigma_\infty \left[\text{Re}\left(\frac{z}{\sqrt{z^2 - L^2}} \right) + x_2 \text{Im}\left(\frac{1}{\sqrt{z^2 - L^2}} - \frac{z^2}{(z^2 - L^2)^{3/2}} \right) \right] \tag{23}$$

where, $z = x_1 + ix_2$. The nonlocal formulation mentioned earlier is applicable for the present problem, since, the crack-surface is stress-free and other boundaries are at infinite distance. Here, using the non-local formulation, the non-local hoop stresses can be obtained numerically using Eq. (4) for a given α (from (20) and (21)). Eringen (2002) has indicated that α may fail to become a function of $\|\boldsymbol{x} - \boldsymbol{x}'\|$ near the crack surface, however, it could be small. Following the same strategy in the current work, the variation of α near the crack surface is neglected. The nonlocal hoop stresses (in Fig. 8(top)) show that the crack-tip behavior is highly dependent on the type of kernel (i.e. on the nature of non-locality). The stress gradient and Gaussian kernels yield crack-tip stress amplification of about 40 and 80 respectively. It is observed that the maximum stress does not occur at the crack-tip but slightly away from it. Since the nonlocal stress is an averaged local stress over the domain of nonlocal influence, at the crack tip, the nonlocal stress is a sum of very low stresses behind the crack and very high stress in front of the crack. This prevents the nonlocal stress from reaching its maximum at the crack-tip. Whereas, slightly away from the crack-tip and in front of it, the local stresses vary from high to very high, leading to a maximum in the nonlocal stress.

The point where the nonlocal stress attains its maximum also depends on the characteristics of the kernel function and the variations in the local stress field. The short-range (sharper) part of the Gaussian kernel has manifold contribution from the nearest zones (within 0.5 Å) than the stress gradient kernel. This weights the sharply varying local stress. As a consequence, the Gaussian kernel shows much higher nonlocal stress near the crack-tip and yields a peak much closer to the crack-tip than that of the stress gradient, see Fig. 8 (middle and bottom). It is evident from the logarithmic plots Fig. 8 (bottom) that away from the crack-tip, the computed nonlocal stresses converge to the classical solution. Going towards the crack-tip, at around 10 Å, the nonlocal hoop stress has the same rate of increase as the classical solution but they are nominally greater due to the nonlocal influence of the higher stresses near the crack. As the distance from the crack-tip decreases further, the nonlocal stresses become significantly greater than the

Please cite this article in press as: Ghosh, S., et al. Non-local modeling of epoxy using an atomistically-informed kernel. Int. J. Solids Struct. (2013), http://dx.doi.org/10.1016/j.ijsolstr.2013.04.025

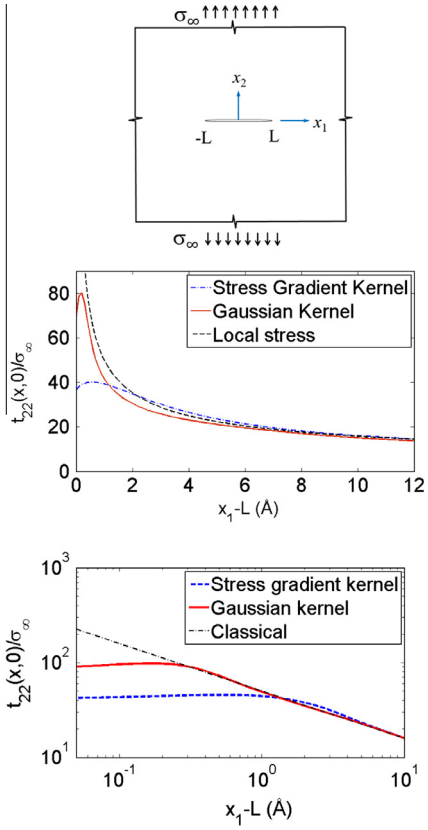

Fig. 8. (top) A Finite crack of length $2L$ (along x_1-axis) in an infinite body loaded in the far field. Crack tip hoop stress along crack line in linear (middle) and logarithmic scale (bottom).

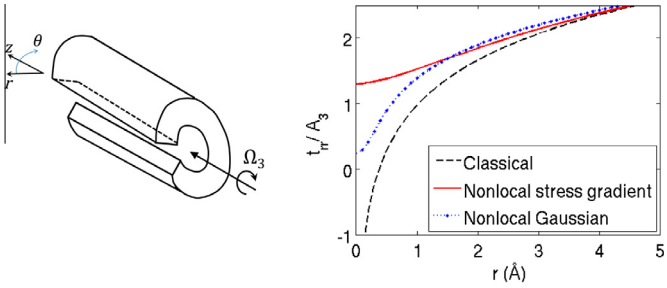

Fig. 9. Straight wedge disclination: (left) schematics (right) t_{rr} along radial line.

classical one. Note that for the Gaussian kernel the nonlocal stress falls below the local stress, at around 2 Å from crack-tip, but it reverts to the trend at 0.7 Å. This fluctuation for the Gaussian kernel is due to two distinct Gaussian bells. As the domain of influence for the long-range (flatter) kernel penetrates the stress-free side of the crack, the nonlocal stress starts to decrease but this effect is eventually countered by the product of the short-range Gaussian and high near-tip stresses. For distances even closer, the nonlocal stress decreases due to influence of the stress-free zones beyond the crack-tip. Also near this point, the nonlocal hoop stress turns away from the inverse-square-root slope of classical elasticity and stays almost flat in a logarithmic scale.

It must be emphasized that the phonon dispersion was obtained using periodic boundary conditions within the MD formulation, that is, the kernels are meaningful for interior part of the body only. Even though the finiteness of stress at the crack-tip is guaranteed due to the nonlocal formalism, the value of stresses within a neighborhood (defined by a sphere of radius r_{cutoff}) of the crack-tip can be estimated only approximately. There exist several purely mathematical approaches to modify the kernel in order to accommodate the effect of the boundary on the nonlocal stress (Polizzotto, 2001; Borino et al., 2003; Polizzotto et al., 2004). However, they are not drawn from material physics related to phonon dispersion at free surfaces.

4.2. Problem of straight disclination

Disclinations are rotational discontinuities, i.e. a defect where the rotational symmetry is violated. Initially they were described by the second class of Volterra dislocations. However, currently they are commonly referred as disclinations following the work of Frank (1958) and Nabarro (1967). Disclinations are used to explain the mechanisms of reorientations, e.g. twinning, kink bands in various materials like liquid crystals, biological structures, large strata of rocks and in other different solids (Povstenko and Matkovskii, 2000). They are an important mode of plastic deformation in polymeric materials such as epoxy as described in Argon theory (Argon, 1975).

In the following, the deformation field due to a straight disclination in an infinite body is considered. The classical elasticity solution for a straight wedge disclination about the z-axis with Frank vector $\Omega = (0, 0, \Omega_3)$ is given by the following equation in a cylindrical polar coordinate system, (r, θ, z) (De Wit, 1973):

$$\sigma_{rr} = A_3\left(ln(r) + \frac{\nu}{1-2\nu}\right), \quad \sigma_{\theta\theta} = A_3\left(ln(r) + \frac{\nu}{1-\nu} + 1\right), \quad \sigma_{r\theta} = 0$$

where, $A_3 = \frac{\mu\Omega_3}{2\pi(1-\nu)}$. The μ, ν denotes shear modulus and Poisson's ratio, respectively.

Fig. 9 shows the radial stresses obtained via classical as well as current nonlocal approach with the atomistically obtained parameters. A logarithmic singularity for the classical elasticity is shown in the equation given above. The nonlocal radial stress, t_{rr}, is obtained by numerically evaluating Eq. (4) for the two kernels. The Gaussian kernel follows the Classical solution more closely near the centre due to the short-range Gaussian component. However, the important aspect of nonlocal elasticity lies in the fact that it avoids the non-physical stress singularity at the centre.

5. Discussion and conclusion

In this paper, we have developed non-local kernels for amorphous polymer (epoxy) using a molecular dynamics-based approach. While phonon dispersion via lattice dynamics is routinely used for crystalline lattices, characterizing phonon behavior for amorphous systems is challenging due to the computational complexity. Here, the key idea is to use the velocity data from equilibrium MD simulations to identify the frequency-wavenumber dispersion response. The vibrational spectrum for a given wave vector is calculated as the Fourier transform of the velocity–velocity autocorrelation function in the reciprocal space. For each wave vector the highest peak of the vibrational spectrum is chosen to obtain the dispersion curve of epoxy. True to the isotropic nature of the epoxy matrix, the longitudinal and transverse dispersion curves for epoxy are seen to fall on a single curve. It was found that the dispersion data deviates from the linear classical elasticity solution and necessitates the need for improved non-local kernels to reproduce this response. Due to the complex vibrational characteristics in the amorphous system, a stress gradient kernel with only one parameter was unable to predict the phonon dispersion. The Gaussian kernel provides a better fit to the dispersion data when two components were employed. The nonlocal kernels are subsequently used within nonlocal elasticity to illustrate its utility in obtaining finite stress values for the crack-tip and disclination

Please cite this article in press as: Ghosh, S., et al. Non-local modeling of epoxy using an atomistically-informed kernel. Int. J. Solids Struct. (2013), http://dx.doi.org/10.1016/j.ijsolstr.2013.04.025

stress fields. A Green's function approach that allows identification of non-local stresses through post-processing of local stress fields is utilized. This work shows how nonlocal elasticity can be used as a multi-scale framework for modeling epoxies with information passed from smaller to higher length scales.

Acknowledgements

The authors would like to acknowledge Boeing Research and Technology for financial support in the project. The authors acknowledge the support of the University of Michigan Center for Advanced Computing (CAC), a high-performance computing center located in the Ann Arbor campus.

Appendix A. Calculating the phonon spectrum

The following will describe the steps to compute the phonon spectrum from a MD simulation. Let $\boldsymbol{r}_i(t)$ and $\boldsymbol{v}_i^p(t)$ are the position and velocity of atom i at time t. The superscript p on the velocity indicates that the motion only in the pth direction is considered. The velocities for an ensemble containing N_a atoms can be projected in reciprocal space to obtain velocity as a function of inverse wavelength ($v_{\boldsymbol{k}}^p$) as given in Eq. (17).

The power spectral density, PSD, $S_x(\omega)$, may be defined as the Fourier transform pair of the autocorrelation function (ACF), $R_x(t)$, for the stochastic process, $x(t)$, (see Wiener–Khinchin theorem (Ricker, 2003; Millers and Childers, 2004)). That is for the stationary stochastic process $v_{\boldsymbol{k}}^p(t)$

$$S_{v_{\boldsymbol{k}}^p}(\omega) = \int_{-\infty}^{\infty} R_{v_{\boldsymbol{k}}^p}(t)\, e^{-i\omega t} dt$$

In the MD approach, the phonon frequencies corresponding to wave vector $\boldsymbol{k}$ was obtained by inspecting the peaks of the PSD. Here, we show that this is indeed the case. Let the Fourier transform of $v_{\boldsymbol{k}}^p(t)$ be denoted as $\hat{v}_{\boldsymbol{k}}^p(\omega)$ and $\hat{v}^{*p}_{\boldsymbol{k}}(\omega)$. Then

$$\hat{v}_{\boldsymbol{k}}\, \hat{v}^*_{\boldsymbol{k}} = \left[\int_{-T/2}^{T/2} v_{\boldsymbol{k}}(t) e^{-i\omega t} dt\right]\left[\int_{-T/2}^{T/2} v_{\boldsymbol{k}}(s) e^{i\omega s} ds\right]$$

where $\hat{v}_{\boldsymbol{k}}^p(\omega)$ and $\hat{v}^{*p}_{\boldsymbol{k}}(\omega)$ are complex conjugate pairs. Note that for brevity the argument, ω, and superscript, p, of $\hat{v}$ has been neglected. Taking expectation

$$\langle \hat{v}_{\boldsymbol{k}}\, \hat{v}^*_{\boldsymbol{k}} \rangle = \int_{-T/2}^{T/2}\int_{-T/2}^{T/2} \langle v_{\boldsymbol{k}}(t) v_{\boldsymbol{k}}(s)\rangle\, e^{-i\omega(t-s)} dt\, ds$$

Setting $s = t + \tau$ and using the definition of ACF

$$\langle \hat{v}_{\boldsymbol{k}}\, \hat{v}^*_{\boldsymbol{k}} \rangle = \int_{-T/2}^{T/2}\int_{-T/2}^{T/2} R_{v_{\boldsymbol{k}}}(\tau)\, e^{-i\omega\tau} dt\, ds$$

using the change of variable formula under the map $\tau = s - t$ and $\eta = s + t$:

$$\begin{aligned}\langle \hat{v}_{\boldsymbol{k}}\, \hat{v}^*_{\boldsymbol{k}} \rangle &= \frac{1}{2}\int_{-T}^{T}\int_{-T+|\tau|}^{T-|\tau|} R_{v_{\boldsymbol{k}}}(\tau)\, e^{-i\omega\tau} d\eta\, d\tau \\ &= T\int_{-T}^{T} R_{v_{\boldsymbol{k}}}(\tau)\, e^{-i\omega\tau}\left(1 - \frac{|\tau|}{T}\right) d\tau\end{aligned}$$

Dividing by T and taking limit for $T \to \infty$:

$$\lim_{T\to\infty} \frac{1}{T}\langle \hat{v}_{\boldsymbol{k}}\, \hat{v}^*_{\boldsymbol{k}} \rangle = \int_{-\infty}^{\infty} R_{v_{\boldsymbol{k}}}(\tau)\, e^{-i\omega\tau} d\tau = S_{v_{\boldsymbol{k}}}(\omega) \tag{24}$$

Therefore the PSD, $S_{v_{\boldsymbol{k}}}(\omega)$, is nothing but $\lim_{T\to\infty} \frac{1}{T}\langle \hat{v}_{\boldsymbol{k}}\, \hat{v}^*_{\boldsymbol{k}} \rangle$, hence it will have peaks at the frequency contents of $\hat{v}_{\boldsymbol{k}}$.

References

Abramowitz, M., Stegun, I.A. (Eds.), 1972. 9.6 in Handbook of Mathematical Functions with Formulas, Graphs, and Mathematical Tables. Dover, New York, 9th printing.
Accelrys Software Inc., Discovery Studio Modeling Environment: Release 5.5, San Diego, 2007.
Aifantis, E.C., 1992. On the role of gradients in the localization of deformation and fracture. International Journal of Engineering Science 30 (10), 1279–1299.
Argon, A.S., 1975. Plastic Deformation in Glassy Polymers, in Polymeric Materials. A.S.M., Metals Park, Ohio, pp. 411–486.
Arroyo, M., Belytschko, T., 2002. An atomistic-based finite deformation membrane for single layer crystalline films. Journal of the Mechanics and Physics of Solids 50, 1941–1977.
Askes, H., Aifantis, E.C., 2011. Gradient elasticity in statics and dynamics: an overview of formulations, length scale identification procedures, finite element implementations and new results. International Journal of Solids and Structures 48 (13), 1962–1990.
Bazant, Z.P., Chang, T-P., 1984. Instability of nonlocal continuum and strain averaging. Journal of Engineering Mechanics 110 (10), 1441–1450.
Borino, G., Failla, B., Parrinello, F., 2003. A symmetric nonlocal damage theory. International Journal of Solids and Structures 40 (13–14), 3621–3645.
Bykztrk, O., Buehler, M.J., Lau, D., Tuakta, C., 2011. Structural solution using molecular dynamics: fundamentals and a case study of epoxy-silica interface. International Journal of Solids and Structures 48 (14–15), 2131–2140.
Chen, C.P., Lakes, R.S., 1989. Dynamic wave dispersion and less properties of conventional and negative poisson's ratio polymeric cellular materials. Cellular Polymers 8, 343–369.
Christensen, S., 2007. Atomistically explicit molecular dynamics simulations of thermosetting polymers. In: Proceedings of 39th ISTC SAMPE Conference.
Dauber-Osguthorpe, P., Roberts, V.A., Osguthorpe, D.J., Wolff, J., Genest, M., Hagler, A.T., 1988. Structure and energetics of ligand binding to proteins: E.coli dihydrofolate reductase-trimethoprim, a drug-receptor system. Proteins: Structure, Function and Genetics 4, 31–47.
De Wit, R., 1973. Theory of disclinations: IV. Straight disclinations. Journal of Research of the National Bureau of Standards 77A, 607.
Dickey, J.M., Paskin, A., 1969. Computer simulation of the lattice dynamics of solids. Physical Review 188 (3), 1407–1418.
DiVincenzo, D.P., 1986. Dispersive corrections to continuum elastic theory in cubic crystals. Physical Review B 34, 5450–5465.
Eringen, A.C., 1972. Linear theory of nonlocal elasticity and dispersion of plane waves. International Journal of Engineering Science 10 (5), 425–435.
Eringen, A.C., 1983. On differential equations of nonlocal elasticity and solutions of screw dislocation and surface waves. Journal of Applied Physics 54 (9), 4703–4710.
Eringen, A.C., 1987. Theory of nonlocal elasticity and some applications. Res Mechanica 21 (4), 313–342.
Eringen, A.C., 2002. Nonlocal Continuum Field Theories. Springer-Verlag, New York.
Eringen, A.C., Edelen, D.G.B., 1972. On nonlocal elasticity. International Journal of Engineering Science 10 (3), 233–248.
Eringen, A.C., Speziale, C.G., Kim, B.S., 1977. Crack-tip problem in non-local elasticity. Journal of the Mechanics and Physics of Solids 25, 339–355.
Frank, F.C., 1958. I. Liquid crystals. On the theory of liquid crystals. Discussions of the Faraday Society 25, 19–28.
Gutkin, M.Y., Aifantis, E.C., 1996. Screw dislocation in gradient elasticity. Scripta Materialia 35 (11), 1353–1358.
Gutkin, M.Y., Aifantis, E.C., 1999. Dislocations in the theory of gradient elasticity. Scripta Materialia 40 (5), 559–566.
Hakobyan, Y., Tadmor, E.B., James, R.D., 2012. Objective quasicontinuum approach for rod problems. Physical Review B 86, 245435.
Han, C-S., 2010. Influence of the molecular structure on indentation size effect in polymers. Materials Science and Engineering: A 527, 619–624.
Heino, P., 2007. Dispersion and thermal resistivity in silicon nanofilms by molecular dynamics. European Physical Journal B 60, 171–179.
Ilcewicz, L.B., Shaar, C., Kennedy, T.C., Wilson, J.B., 1986. Experimental evidence of a relationship between ultrasonic wave dispersion and fracture. Engineering Fracture Mechanics 24 (6), 895–908.
Jiang, L., Tan, H., Wu, J., Huang, Y., Hwang, K.-C., 2007. Continuum modeling of interfaces in polymer matrix composites reinforced by carbon nanotubes. Nano 2 (03), 139–148.
Kunin, I.A., 1982. Elastic Media with Microstructure I. Springer, Berlin.
Lam, D.C.C., Yang, F., Chong, A.C.M., Wang, J., Tong, P., 2003. Experiments and theory in strain gradient elasticity. Journal of the Mechanics and Physics of Solids 51 (8), 1477–1508.
Lau, D., Bykztrk, O., Buehler, M.J., 2012. Characterization of the intrinsic strength between epoxy and silica using a multiscale approach. Journal of Materials Research 27 (14), 1787–1796.
Maranganti, P., Sharma, R., 2007. A novel atomistic approach to determine strain gradient elasticity constants: tabulation and comparison for various metals, semiconductors, silica, polymers and the (ir) relevance for nanotechnologies. Journal of the Mechanics and Physics of Solids 55 (9), 1823–1852.
Miller, R.E., Tadmor, E.B., 2009. A unified framework and performance benchmark of fourteen multiscale atomistic/continuum coupling methods. Modelling and Simulation in Materials Science and Engineering 17, 053001.
Millers, S., Childers, D., 2004. Probability and Random Processes. Elsevier Academic Press, London.

Please cite this article in press as: Ghosh, S., et al. Non-local modeling of epoxy using an atomistically-informed kernel. Int. J. Solids Struct. (2013), http://dx.doi.org/10.1016/j.ijsolstr.2013.04.025

Nabarro, F.R.N., 1967. Theory of Crystal Dislocations. Oxford University Press, London.
Picu, R.C., 2002. On the functional form of non-local elasticity kernels. Journal of the Mechanics and Physics of Solids 50 (9), 1923–1939.
Polizzotto, C., 2001. Nonlocal elasticity and related variational principles. International Journal of Solids and Structures 38, 7359–7380.
Polizzotto, C., Fuschi, P., Pisano, A.A., 2004. A strain-difference-based nonlocal elasticity model. International Journal of Solids and Structures 41, 2383–2401.
Povstenko, Y.Z., Matkovskii, O.A., 2000. Circular disclination loops in nonlocal elasticity. International Journal of Solids and Structures 37, 6419–6432.
Ricker, D.W., 2003. Echo Signal Processing. Springer.
Ru, E.C., Aifantis, C.Q., 1993. A simple approach to solve boundary-value problems in gradient elasticity. Acta Mechanica 101 (1–4), 59–68.
Silling, S.A., 2000. Reformulation of elasticity theory for discontinuities and long-range forces. Journal of the Mechanics and Physics of Solids 48, 175–209.
Sundararaghavan, V., Kumar, A., 2013. Molecular dynamics simulations of compressive yielding in crosslinked epoxies in the context of argon theory, International Journal of Plasticity. in press, http://dx.doi.org/10.1016/j.ijplas.2013.01.004.
Sundararaghavan, V., Waas, A.M., 2011. Non-local continuum modeling of carbon nanotubes: physical interpretation of non-local kernels using atomistic simulations. Journal of the Mechanics and Physics of Solids 59 (6), 1191–1203.
Tadmor, E.B., Ortiz, M., Phillips, R., 1996. Quasicontinuum analysis of defects in solids. Philosophical Magazine A 73 (6), 1529–1563.
Tan, V.B., Zeng, X.S., Deng, M., Lim, K.M., Tay, T.E., 2008. Multiscale modeling of polymers – the pseudo amorphous cell. Computer Methods in Applied Mechanics and Engineering 197, 536–554.
Tcharkhtchi, A., Gouin, E., Verdu, J., 2000. Thermal expansion of epoxide amine networks in the glassy state. Journal of Polymer Science: Part B: Polymer Physics 38, 537–543.
Varshney, V., Patnaik, S.S., Roy, A.K., Farmer, B.L., 2008. A molecular dynamics study of epoxy-based networks: cross-linking procedure and prediction of molecular and material properties. Macromolecules 41, 6837–6842.
Wang, Q., Storm, B.K., Houmoller, L.P., 2003. Study of the isothermal curing of an epoxy prepreg by near-infrared spectroscopy. Journal of Applied Polymer Science 87, 2295–2305.
Zhang, P., Jiang, H., Huang, Y., Geubelle, P.H., Hwang, K.C., 2004. An atomistic-based continuum theory for carbon nanotubes: analysis of fracture nucleation. Journal of the Mechanics and Physics of Solids 52, 977–998.

Please cite this article in press as: Ghosh, S., et al. Non-local modeling of epoxy using an atomistically-informed kernel. Int. J. Solids Struct. (2013), http://dx.doi.org/10.1016/j.ijsolstr.2013.04.025